

Development of an in-vacuum minipole undulator array for National Synchrotron Light Source In-Vacuum UNdulator

T. Tanabe,^{a)} X. Marechal, T. Tanaka, and H. Kitamura
JAERI-RIKEN SPring-8 Project Team, Kamigori, Ako-gun, Hyogo 678-12, Japan

P. Stefan, S. Krinsky, G. Rakowsky, and L. Solomon
National Synchrotron Light Source, Brookhaven National Laboratory, Upton, New York 11973

(Received 2 September 1997; accepted for publication 28 September 1997)

An in-vacuum minipole (short period) insertion device has been developed in a collaboration between SPring-8 and the National Synchrotron Light Source (NSLS). The magnetic arrays were assembled, field measured, corrected, and vacuum tested by SPring-8 and were installed in an NSLS-developed chamber with mechanical parts in the NSLS X-Ray Ring ($E = 2.584$ GeV) in May 1997 and a successful commissioning of the device was carried out in June 1997. The device is made of permanent magnets with 30.5 periods and a period length of 11 mm. It is designed to produce fundamental radiation at 4.6 keV, and with a modest value of deflection parameter ($K = 0.7$ at 3.3 mm gap) enables higher harmonics to be used as well, for a variety of experiments. A detailed description of the mechanical support and vacuum chamber will be reported elsewhere. We describe technical challenges encountered in constructing this type of device, and present an outline of our collaboration. © 1998 American Institute of Physics. [S0034-6748(98)04601-2]

I. INTRODUCTION

As a convention, a so-called “minipole” undulator refers to an insertion device (ID) with a period length of the order of 1 cm or less. Various minipole undulators have been developed for linac use, mainly because the small magnet gap required for this type of device would prevent its use in storage rings. However, with the advent of the third generation light source, the vertical emittance of the electron beam (e -beam) has become small enough to accommodate subcentimeter magnet gaps without sacrificing e -beam lifetime. Unlike conventional insertion devices, whose minimum gap is limited by the vertical size of the vacuum chambers, in-vacuum insertion devices allow the magnetic gap to be closed to the beam dynamics limit. This advantage is even more crucial for minipole devices, which inherently require a smaller magnet gap than conventional devices, in order to increase the undulator deflection parameter K . With a value of K not much smaller than unity, the use of higher harmonics and modest tunability are possible.

In Sec. II, we describe the aim of this collaboration, and some attention is given to the characteristics of National Synchrotron Light Source (NSLS) X-Ray Ring, as well as ID parameters. The effect of emittance on the radiation spectrum is also discussed. Design details of the magnet blocks and holder structure are reported in Sec. III. Permeance of the magnetic circuit is one subject which calls for particular attention. Section IV is devoted to magnetic field measurement and field correction of the device. Both spectral and multipole characteristics are thoroughly examined. Vacuum testing of the array is detailed in the following section and the concerns of ring impedance in the transition areas is discussed in Sec. IV.

II. NSLS-IN-VACUUM UNDULATOR (IVUN) PROJECT

The use of in-vacuum minipole undulators in a medium-sized ring (a few GeV) is a good alternative to relying on a large-scale facility such as the European Synchrotron Research Facility (ESRF), the Advanced Photon Source (APS), or SPring-8 to obtain undulator photons in the 10 keV range. The technology of the in-vacuum insertion device was first developed at Kou Enerugi Kenkyusho (KEK)¹ and later refined at SPring-8, where a commitment to extensive use of them has been made.² As a part of a research activity into future SPring-8 devices, we have collaborated in the development of a device called NSLS-IVUN which was installed in the X-Ray Ring ($E = 2.584$ GeV) at the National Synchrotron Light Source (NSLS) in Brookhaven National Laboratory (BNL) in May 1997. The magnetic arrays were developed by SPring-8 and they are installed in a vacuum chamber with mechanical and control systems developed at the NSLS.

NSLS x-ray ring parameters as of May 1997 are given in Table I. Despite the fact that this ring is a second-generation light source, extremely low beam coupling ($\sim 0.1\%$) enables us to achieve a minimum-gap operation of 2.5 mm. The predicted radiation spectra for the IVUN with zero emittance and zero beam-energy spread and, with the actual finite values are shown in Fig. 1. Tuning capability of the device can be seen in Fig. 2, in which peak brilliance as a function of K is shown. As can be seen in Fig. 1, although horizontal emittance degrades the brilliance of the radiation, it makes the use of the second harmonic on-axis possible. An improved lattice has been designed for future use at NSLS, with which the brilliance increases by a factor of two.

III. DESIGN OF THE MAGNET ARRAYS

An in-vacuum minipole undulator imposes extra constraints and challenges compared to conventional IDs in design of the magnet arrays primarily due to the following: (1)

^{a)}Present address: RI Beam Factory Project, The Institute of Physical and Chemical Research (RIKEN), 2-1 Hirosawa, Wako, Saitama 351-01, Japan; electronic mail: ttanabe@postman.riken.go.jp

TABLE I. Pertinent NLS x-ray ring parameters for IVUN operation.

	Operations lattice	Low emittance lattice (in future)
Energy	2.584 GeV	←
Max current	430 mA	?
β_x/β_y	1.70 m/0.37 m	1.17 m/0.30 m
$\eta_x/\eta_{x'}$	-0.088/0.04	0.17/0
α_x/α_y	0.23/-0.02	-0.002/0
σ_E/σ_L (FWHM)	0.085%/13 cm	←
ϵ_x/ϵ_y	94 nm rad/0.1 nm rad	45 nm rad/0.1 nm rad
σ_x/σ_y	407 μm /6.2 μm	271 μm /5.6 μm
$\sigma_{x'}/\sigma_{y'}$	244 μrad /16.7 μrad	196 μrad /18.6 μrad

Higher machining accuracy is required, simply because of the small physical dimensions. (2) As the minimum allowable size of the good-field region (horizontal field roll off less than 0.5%) for stable ring operation remains the same as in a conventional device, the horizontal dimension of the magnet cannot be decreased beyond a certain value. (3) Due to the in-vacuum bakeout required of the magnets, the permeance of magnet blocks in the magnetic circuit should not be lower than a critical value which could lead to excessive demagnetization. In general, stocky pieces are more favorable than thin ones, which contradicts requirement (2). Each factor will be examined below.

A. Machining accuracy and mechanical design

Even if the magnetic material were made completely uniform, machining errors in magnet blocks and holders would contribute errors in the magnetic field strength and trajectory phase. As the period length decreases, the relative errors increase for a given machining accuracy. Variation in the thickness of the titanium nitride (TiN) coating, which helps reduce degassing from the magnetic material, also contributes to block size errors. A construction scheme with individual, independent magnet holders and clamps is not appropriate, as relative errors in machining with respect to the block size become larger and the large number of gaps created by this structure may result in poor vacuum perfor-

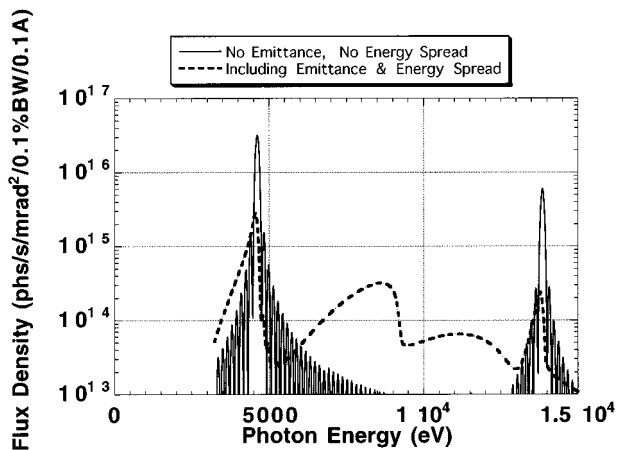


FIG. 1. Calculated flux density for IVUN. The solid line indicates the flux density from an electron beam without emittance and energy spread. The broken line represents predicted values including these effects.

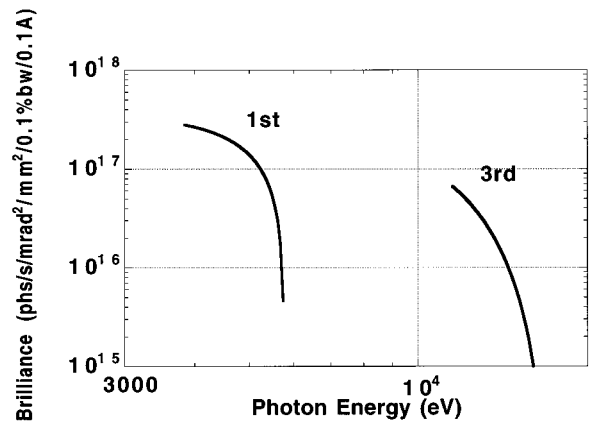


FIG. 2. Tuning capability in the fundamental wavelength and the third harmonic of IVUN. K values are varied from 1 to 0.1.

mance. Hence, we have developed a novel structure to place and hold small magnet pieces in precise locations, and it is depicted in Fig. 3. A newly developed neodymium-iron-boron magnet material with a very high intrinsic coercivity (NEOMAX 32EH) was used. Errors in periodicity are considered important, as they cannot be corrected later, unlike field strength errors. In this structure, the accuracy of the side plate period is the determining factor, and it is made to be within $\pm 10 \mu\text{m}$ by computer-aided machining. The thickness variation of the $5 \mu\text{m}$ thick TiN coating is less than $1 \mu\text{m}$. The base plates and side plates are made of Al 2219-T852, which is a good match for the Al 2219-T87 that the NLS uses for the support structure. Ideally, the array units and support should be made from identical materials but Al 2219-T87 was not available in small sizes in Japan. We have not experienced any problem caused by this difference so far. The small clamps are made of BeCu and have a springlike feature, to ensure that the clamping forces are equally applied to all four blocks beneath. It became clear later that this structure required additional improvement as some clamps were twisted, which caused a few magnet blocks to break. This problem was alleviated once all the screws were removed and retorqued evenly.

The $100 \mu\text{m}$ Ni foil covers the magnet array surface in order to reduce the resistive impedance contribution of the device. Magnetically the effect of this thin foil is small at a

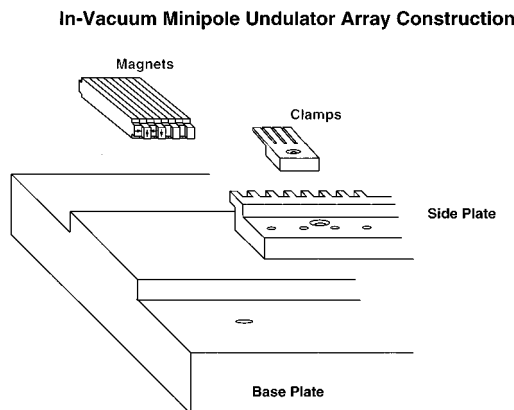


FIG. 3. Schematic picture of the IVUN array structure.

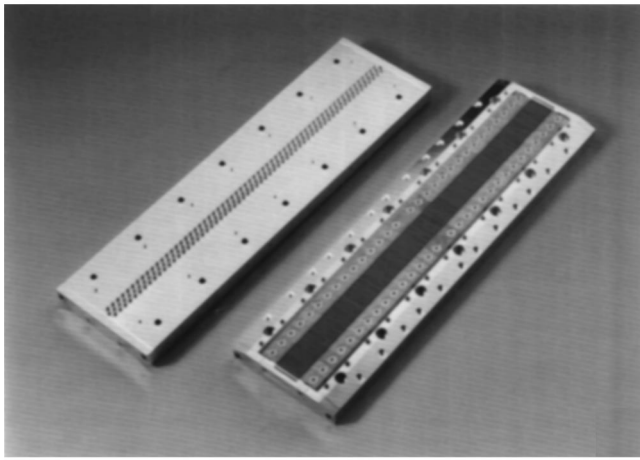


FIG. 4. A photograph of the IVUN array units.

3.3 mm gap, magnetic field reduction was only 20 to 30 G out of 7000 G peak and no excessive field distortion was observed. Ni was chosen because of its relatively high electrical conductivity to reduce resistive impedance, its UHV compatibility, and its magnetic nature to secure attachment to the magnet surface. Figure 4 is a picture of fabricated array units, without Ni sheets, taken before shipment to BNL.

B. Good field region

The good field region of an insertion device is an arbitrary concept and is usually defined as a horizontal region in which the magnetic field varies less than 0.5% from the peak value at the center. For Halbach-type structures, it is almost entirely determined by the horizontal size of magnet blocks. At the x-ray ring of the NSLS, a good-field region of at least ± 5 mm was required. As shown in Fig. 5, the minimum horizontal size for IVUN to satisfy this condition is 22 mm. Therefore, the other two block dimensions have to be determined by a combination of factors, such as the required period length and K value and the minimum allowable value for the permeance of the magnet blocks.

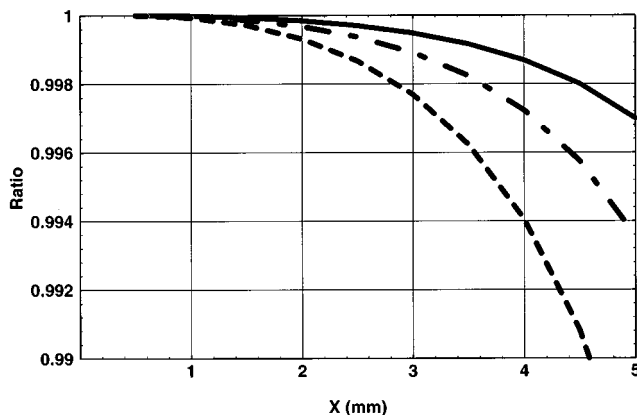


FIG. 5. Field roll off due to finite width (gap=3.3 mm). The height of the magnet block is 3.92 mm, and the width of the magnet is 20 mm (broken-dotted line), 18 mm (broken line), and 15 mm (solid line).

C. Demagnetization characteristics of the magnet blocks

Permeance is the ratio of the local magnetic flux density in the magnet to the local demagnetization field.³ It is related to the tendency of the magnet to demagnetize under an external stress, such as heat. The higher the value of the permeance, the less prone the magnet is to demagnetize. Permeance depends on the shape of the magnet piece and the structure of the magnetic circuit. In general, the less out stretched the piece is, the higher the average value of its permeance. Figures 6(a) and 6(b) show contour plots of the calculated permeance values in the horizontal half of the vertically magnetized block (VMB) (a) at a 5 mm gap and (b) at a 2 mm gap, respectively. Similarly, Figs. 6(c) and 6(d) are for a horizontally magnetized block (HMB), (c) at a 5 mm gap and (d) at a 2 mm gap. All these plots were calculated using the integral element method (ELF-MAGIC, ELF.) They indicate that the HMBs have, on average, lower values of permeance, so that they become the limiting factor to a reduction in magnet size. Also, the permeance is lower with larger gaps, so a smaller gap should be maintained during bake-out, in order to minimize demagnetization. It can also be inferred, from the fact that the major part of the magnetic flux in an HMB goes to the side of the magnet away from the gap, and that the vertical size of the HMBs could be reduced without sacrificing maximum flux, while improving the demagnetization characteristics.

IV. MAGNETIC FIELD MEASUREMENT AND FIELD CORRECTION

A photograph of our magnetic field measurement facilities is shown in Fig. 7. There are two types of systems: (1) a Hall probe field mapping system, which includes a moving stage on a granite bench, holders for magnet arrays, and a base plate, and (2) a rotating coil field integral measurement system, which is seen in the upper right corner of the picture.

A. Magnetic measurement bench with Hall probe

The Hall probe used is the AREPOC HHP-MP, which has an active area of $100 \mu\text{m} \times 100 \mu\text{m}$, and an enclosure thickness of 1 mm. It is placed in a 1.5-mm-thick copper plate with duralumin support arm and sandwiched with Kapton tape. Calibration was done in house using a nuclear magnetic resonance (NMR) probe and a standard dipole electromagnet. Even though there is no temperature controlling device in the enclosure of the probe, the low temperature coefficient of the probe ($3.0 \times 10^{-4}/\text{K}$), software compensation and reasonable ambient temperature control ensure the accuracy of the measurements. Extra attention was paid to the straightness and flatness of the probe travel. The granite bench and the supports holding the arrays sit on a single stainless base plate, 5 cm thick. The center of the probe has been found to stay on axis within a range of $\pm 1 \mu\text{m}$ vertically, and $\pm 7 \mu\text{m}$ horizontally through the travel. For the longitudinal direction, the maximum deviation from the ideal position has also been measured using a laser interferometer and was found to be within $15 \mu\text{m}$ for 500 mm travel.

A stepping motor (UPD544HG1-NB, Oriental Motor)

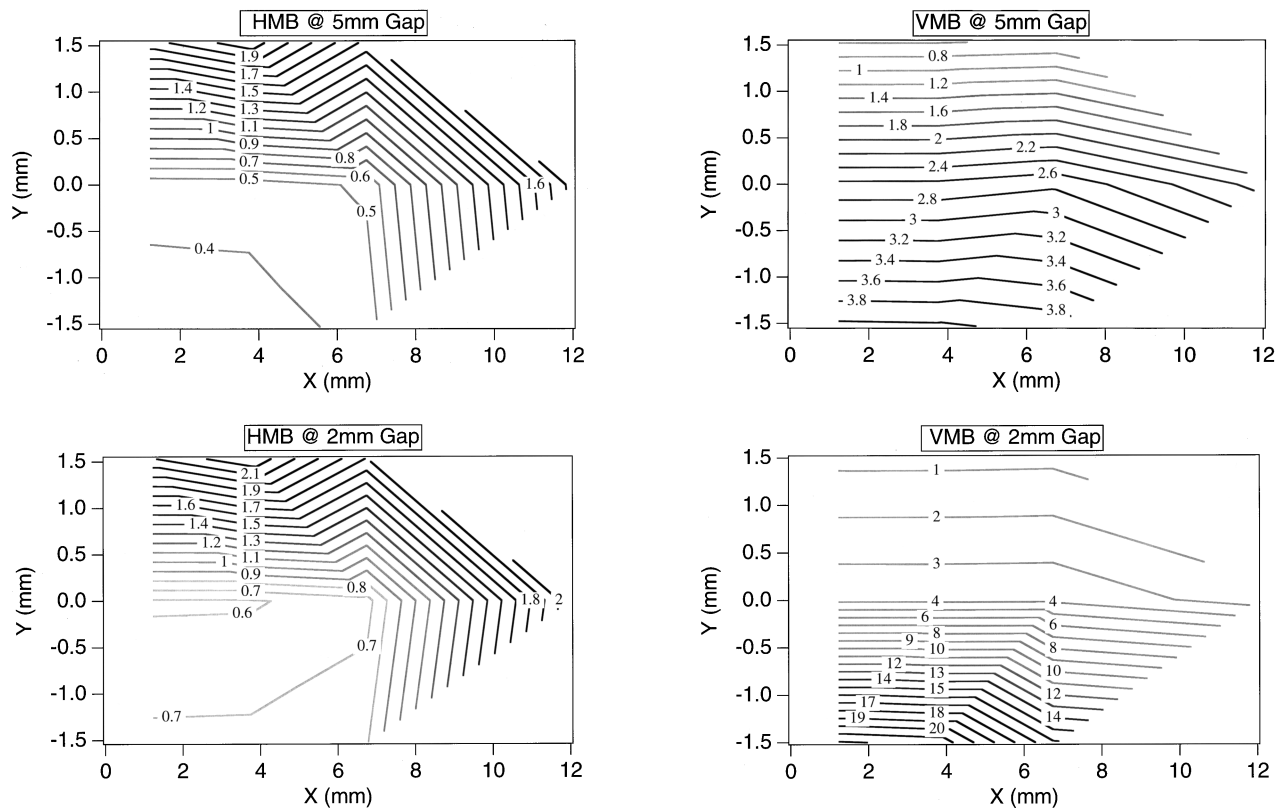


FIG. 6. Contour plot of permeance values in the array; (a) horizontally magnetized block at a gap of (a) 5 mm, (b) 2 mm vertically magnetized block at a gap of (c) 5 mm, (d) 2 mm.

drives a high precision ball screw on which both x and y stages are laid. The motor controller (Sigma Mark-41, Sigma Kohki) is connected to a personal computer (PC) by a General Purpose Interface Bus (GPIB) interface and the data acquisition program is written in LABVIEW (Ver. 3.1, National Instruments). In the software, the probe output voltage is compensated using the temperature difference between probe calibration and that at the time of measurement.

B. Rotating coil system

A conventional flipping coil system⁴ employs multturn coils whose output goes to an integrator or programmable

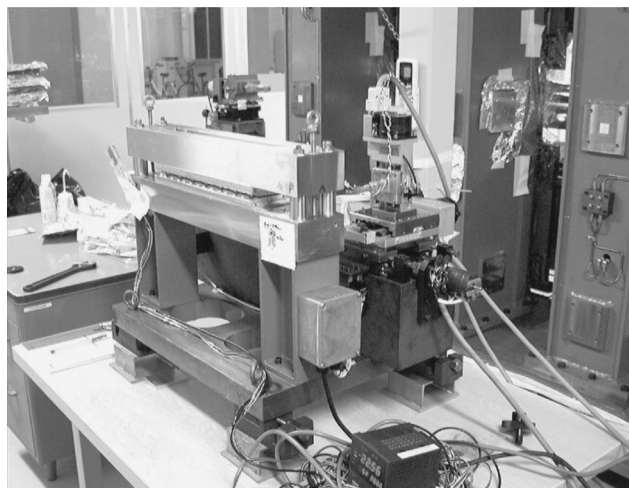


FIG. 7. A photograph of the magnetic measurement facility.

voltmeter for integration. The coil usually has a limited range of rotation, and integration must be done within this range. As a consequence, all the frequency components of the output voltage from the coil are included and noise filtration becomes a major obstacle.

One of the most effective means for noise reduction is to limit the bandwidth of the measurement. In order to apply this method to a flipping coil system, one needs a connector which enables the rotation of the coil while maintaining electrical contact. The rotary connector used (Mercotac Model 205) fulfills this condition by having mercury as an electrical interface medium. A lock-in amplifier is used to measure the coil output, and both normal and skew components of the first integral can be measured simultaneously as the two quadratures. The first integral I_y and I_x could be derived from the following equation;

$$V = Nd\omega(I_y \sin \omega t + I_x \cos \omega t) = A \cos(\omega t - \phi), \quad (1)$$

where V is the induced voltage from the coil, N is the number of coil turns, d is the coil width, and ω is the angular frequency of the rotation. The lock-in amplifier measures A and ϕ . The second integral could be calculated using a crossed coil⁵

$$\theta_x = -\phi_x / \Theta + L \cdot I_x, \quad (2)$$

where $\Theta = d/L$, d : whole width of the coil, L : a half length of the coil, and ϕ_x is the coefficient of the sine component of the integrated flux. The same expression applies to the y component by changing the subscript from x to y .

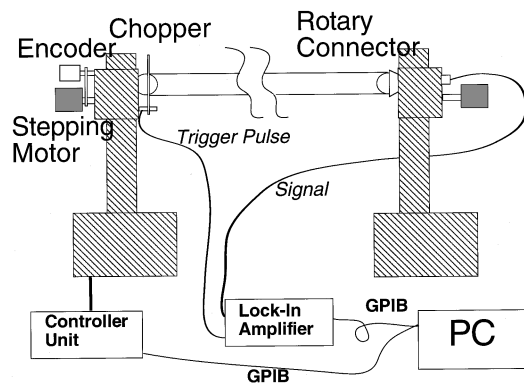


FIG. 8. A schematic picture of the rotating coil device.

Figure 8 shows a schematic of the system layout. Two stepping motors (Oriental Motor UPK-569-NAC) rotate the coil at 5 Hz. The motor controller (Tsuji Denshi Flip-Coil-Controller) ensures synchronization of the two motors to better than 0.1° . The absolute rotary encoder (K+R CE-65-P) has 3600 divisions per turn while the minimum motor step is 0.1° . The multiturn coil is made of Teflon[®] coated tungsten wire (Nippon Tungsten) of 0.1 mm in diameter. The coil width is 1.5 mm with four turns and the length is 1.6 m. Copper wire was deemed unsuitable, as a rather high tension (1 kgf/wire) is required to maintain a constant width of the coil during rotation at five turns per second. We could observe a steady increase in the output voltage during the measurement, due to the stretching of the wire and subsequent increase of the coil area when 0.2 mm-diam enameled copper wire was initially used. A lock-in amplifier (Stanford Research SR850) with a diagonal signal processor (DSP) was used, and the advantage of a very low minimum detectable frequency (1 mHz). It also has a very high dynamic reserve, compared to a conventional analog unit so that use of an electrical noise filter could be avoided.

Field correction was made by first using simulated annealing⁶ for coarse correction, then inserting magnet chips against the back surfaces of the magnet blocks for fine adjustment. This procedure has been found effective for SPring-8 in-vacuum undulators. A stainless steel chip of the same shape as the chip magnet is always inserted between the main magnet and chip magnet to permit removability. The multipole components are measured within a range of $x = \pm 4$ mm. They are derived from a polynomial fit of the first integral distribution along the transverse horizontal axis using the following formula.

TABLE II. Integrated multipole goals for the NSLS x-ray ring and measured results for the IVUN arrays measured at SPring-8.

	Measured results	Goal
Normal/skew dipole	77/-70 G*cm	100 G*cm
Normal/skew quadrupole	25 G/-192 G	10 G/100 G
Normal/skew sextupole	161/41 G/cm	50 G/cm
Normal 2nd integral	0.031 G*m ²	8 G*m ²
Skew 2nd integral	N.A.	8 G*m ²
rms phase shake	1.45°	2°

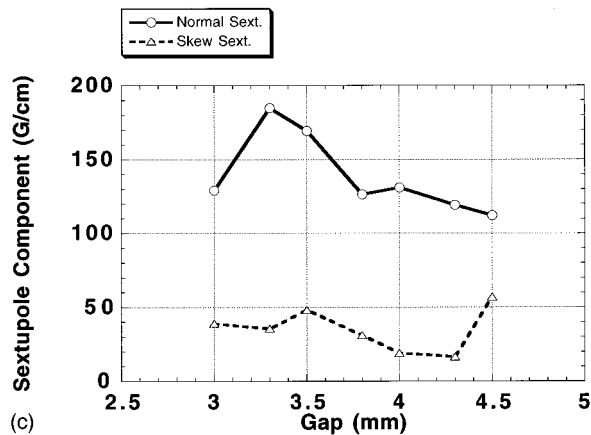
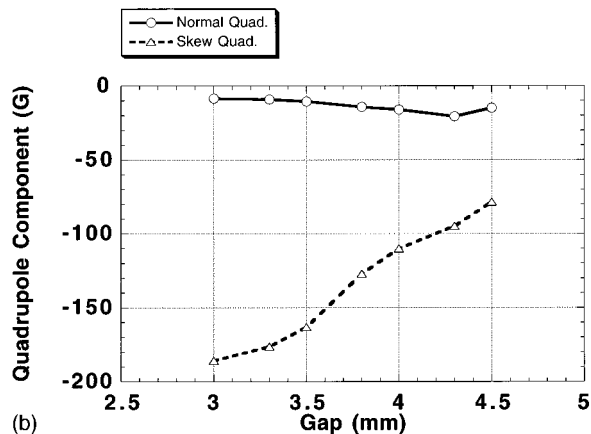
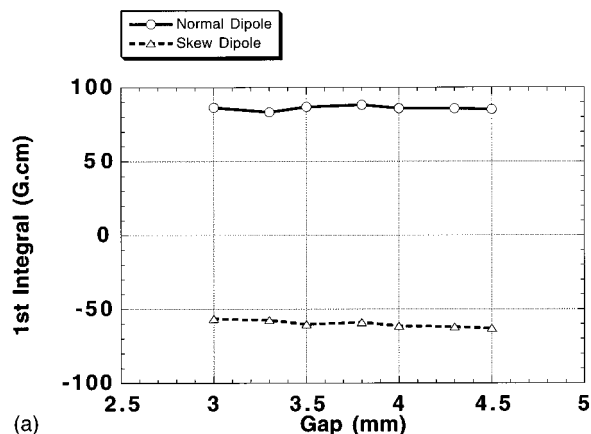


FIG. 9. Gap dependence of integrated multipole components: (a) dipole, (b) quadrupole, and (c) sextupole.

$$\int_{-\infty}^{\infty} (B_y + iB_x) dz = \sum_{n=0}^{\infty} (b_n + ia_n)(x + iy)^n, \quad (3)$$

where b_n is the normal components and a_n as the skew components. Integrated multipole requirements for the NSLS X-Ray Ring and our measurement results are presented in Table II.

Field correction was made in two steps. First, the trajectory on axis was optimized, then multipole correction by chip magnets was performed mostly at the last few periods, to avoid trajectory deviation. At one point, we found out that a major multipole correction was necessary and decided to

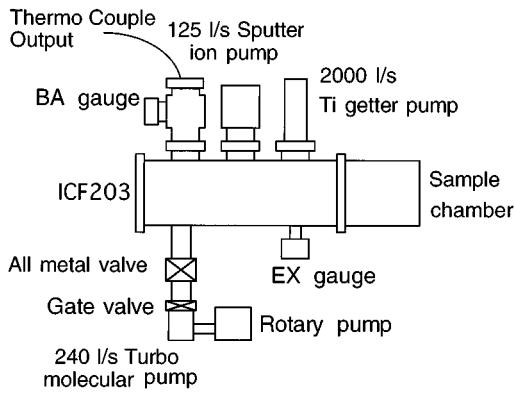


FIG. 10. A schematic of the vacuum test facility.

rotate several magnet blocks by 180° along the y axis. These magnets were chosen based on the results of field mapping with the Hall probe. With hindsight, it would have been better if any necessary repositioning of magnet blocks had been performed before any correction. Figures 9(a)–9(c) show the gap dependence of the final values of the integrated dipole, quadrupole, and sextupole components, respectively. It appears that determining the sextupole components is more sensitive to curve-fitting errors.

V. ULTRAHIGH VACUUM TESTING

After magnetic field correction was finished, a vacuum test in a UHV minichamber was conducted to make sure that no objectionable elements degas from the magnet arrays. A schematic of the vacuum testing facility is given in Fig. 10. The chamber is equipped with a 125 ℓ /s ion pump and a 200 ℓ /s titanium sublimation pump in addition to a 240 ℓ /s turbo molecular pump and rotary pump which were used for initial pump down. The 105-cm-long chamber has an inner diameter of 14.7 cm and is sealed with an ICF203 at one end. The other end is connected to a sample chamber, 50 cm long. The array units are held to form a real magnetic circuit inside the sample chamber. The temperature of the magnets did not exceed 125° . Three types of vacuum gauges were used, cold cathode gauge (CCG) for low vacuum, Bayard Alpert nude gauge (BAG), and Extractor gauge (EXG) for UHV. Figure 11 shows pressure readings from the various gauges versus elapsed time. The difference between the reading of the BAG and that of the EXG in the final hours comes from the fact

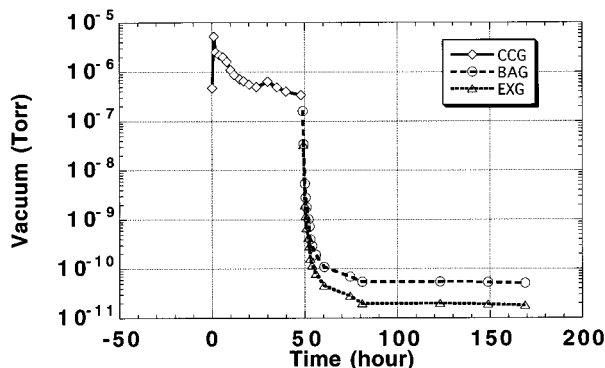


FIG. 11. Pressure readings from the various gauges vs the elapsed time.

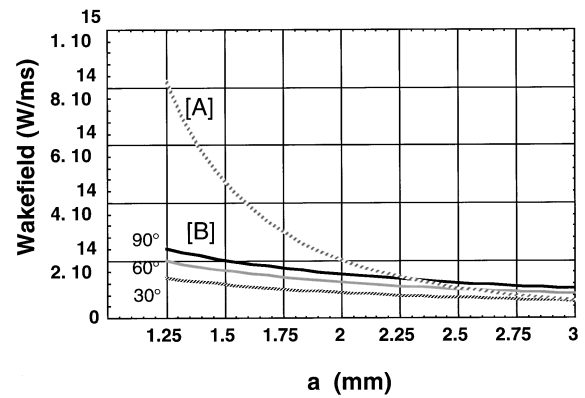


FIG. 12. Wake field created by (a) the transverse resistive impedance and (b) the transverse geometric impedance with different entrance angles (30° , 60° , and 90°).

that the BAG has approached its x-ray limit while, the EXG limit is still lower. The final value reading by the EXG (IONIVAC IM520, Leybold) was 2×10^{-9} Pa, which implies adequate ultrahigh-vacuum (UHV) compatibility of the arrays.

VI. TRANSITION REGIONS

According to Ref. 7, there are three predominant beam dynamic effects caused by the small gap aperture of the minipole undulator and the aperture change due to transitions from the standard vacuum chamber to the ID. They are: power dissipation due to longitudinal impedance and transverse coupled bunch instability/strong head-tail instability caused by transverse resistive impedance and transverse geometric impedance.

Power dissipation can be estimated from Eq. (2.4) in Ref. 7, when an average current I_{av} is distributed uniformly in M bunches and the half aperture is a mm,

$$P \approx M \left(\frac{I_{av}}{M} \right)^2 \left(\frac{1}{2\pi a} \right) \left(\frac{\rho}{\delta_0} \right) \left(\frac{R}{\sigma_s} \right)^{3/2}, \quad (4)$$

where “ l ” is the chamber length, “ R ” is effective radius of the ring, “ σ_s ” is bunch length, “ ρ ” is the resistivity of the chamber material, and “ δ_0 ” is the skin depth in the chamber. For a stainless surface with a 1 mm half aperture and single bunch e -beam current of 0.1 A, it is only 19 W. The only concern here is the possibility that the continuity sheet is detached from the magnet array so that the heat is dissipated by radiation alone. For this reason, we decided to use a thin Ni sheet which, even though Ni is ferromagnetic, it is so thin (100 μm) that the material is easily magnetically saturated and the shunt effect is almost negligible.

The maximum value of the wakefield from a Gaussian bunch due to transverse resistive impedance can be calculated from Eq. (2.17) in Ref. 7,

$$W_{\perp res} = (1.28) \times \frac{2}{\pi a^3} \sqrt{\frac{c\rho}{4\pi\epsilon_0}} \sqrt{\frac{2}{\pi\sigma_s}} \quad (5)$$

and transverse geometric wakefield also given in Eq. (3.1) in Ref. 7,

$$W_{\perp \text{geo}} = \frac{Z_0 c}{\pi a} \left(\frac{2\theta}{\pi} \right)^{1/3} \frac{1}{\sqrt{2\pi\sigma_s}}, \quad (6)$$

where θ is the taper angle from the standard chamber to the small gap and $Z_0 = 377 \Omega$.

Figure 12 plots Eqs. (5) and (6) with three different angles. It appears that at a gap smaller than 2 mm, the transverse resistive impedance becomes dominant, as it is inversely proportional to the third power of the gap, whereas the geometric wakefield goes as the inverse first power. These transverse effects are comparable when the undulator is operated at a gap of 3.3 mm. Tapering the transition section to reduce the geometric effect may not significantly improve the situation.

ACKNOWLEDGMENTS

One of the authors (T. Tanabe) wishes to thank S. Okada and T. Kohda of Sumitomo Special Metals Co. for their support.

¹S. Yamamoto, T. Shioya, M. Hara, H. Kitamura, X. W. Zhang, T. Mochizuki, H. Sugiyama, and M. Ando, *Rev. Sci. Instrum.* **63**, 400 (1992).

²Insertion Device Handbook '96 (SPRING-8 OPSRR 1996-0003).

³R. J. Parker, *Advances in Permanent Magnetism* (Wiley-Interscience, New York, 1990).

⁴See for example, R. P. Walker, *Magnetic Measurement, Synchrotron Radiation Sources* (World Scientific, Singapore, 1994).

⁵D. Frachon, I. Vasserma, P. M. Ivanov, E. A. Medvedko, E. Gluskin, and N. A. Vinolurov, ANL/APS/TB-22 (1995).

⁶A. Cox and B. Youngman, *Proc. SPIE* **582**, 91 (1986).

⁷K. Bane and S. Krinsky, BNL Informal Report, BNL-48792 (1993).